Journal of Applied Polymer Science

Mechanical and Thermal Properties of Bio-Based $CaCO_3$/Soybean-Based Hybrid Unsaturated Polyester Nanocomposites

Tarig A. Hassan, Vijaya K. Rangari, Shaik Jeelani
Department of Materials Science and Engineering, Tuskegee University, Tuskegee, Alabama 36088
Correspondence to: V. K. Rangari (E - mail: rangariv@mytu.tuskegge.edu) or T. A. Hassan (E - mail: hassant@mytu.tuskegee.edu)

ABSTRACT: Bio-based calcium carbonate nanoparticles ($CaCO_3$) were synthesized via size reduction of eggshell powder using mechanical attrition followed by high intensity ultrasonic irradiation. The transmission electron microscopic (TEM) and BET surface area measurements show that these particles are less than 10 nm in size and a surface area of ~44 m^2/g. Bio-based nanocomposites were fabricated by infusion of different weight fractions of as-prepared $CaCO_3$ nanoparticles into Polylite® 31325-00 resin system using a non-contact Thinky® mixing method. As-prepared bio-nanocomposites were characterized for their thermal and mechanical properties. TEM studies showed that the particles were well dispersed over the entire volume of the matrix. Thermal analyses indicated that the bio-nanocomposites are thermally more stable than the corresponding neat systems. Nanocomposite with 2% by weight loading of bio-$CaCO_3$ nanoparticles exhibited an 18°C increase in the glass transition temperature over the neat Polylite 31325 system. Mechanical tests have been carried out for both bio-nanocomposites and neat resin systems. The compression test results of the 2% Bio-$CaCO_3$/Polylite 31325 nanocomposite showed an improvement of 14% and 27% in compressive strength and modulus respectively compared with the neat system. Details of the fabrication procedure and thermal and mechanical characterizations are presented in this article. © 2013 Wiley Periodicals, Inc. J. Appl. Polym. Sci. 130: 1442–1452, 2013

KEYWORDS: mechanical properties; manufacturing; thermosets; thermal properties; biomaterials

Received 1 November 2012; accepted 24 February 2013; published online 17 April 2013
DOI: 10.1002/app.39227

INTRODUCTION

Nanostructured materials have been extensively used as fillers in the manufacturing of composite materials for many engineering applications because of their unique properties. These nanofiller-infused polymer systems exhibit enhanced properties as compared with neat polymers.[1,2] Recently, growing efforts have emerged to develop new classes of bio-inspired composite materials. The main advantage of these types of materials is that they are environmentally friendly and does not contribute to the depletion of energy resources because they are derived from renewable resources. Reasons for this development also include the continuous increase in the prices of oil-derived products along with their destructive effects on the environment.[3] Researchers have developed a broad range of chemical routes to use bio-based and natural materials such soybean oil in creation of biopolymers and composites.[4–7] These materials have economic and environmental advantages over the petroleum-based materials that make them attractive alternatives in a wide range of applications. The significant enhancement of thermal and mechanical properties of these materials at low loadings of bio-nanofillers highlights the importance of this new class of bio-based polymer composites for industrial applications. In particular to the automotive sector where the continued need for material weight reduction must always be balanced with consideration of structural requirements and environmental friendly.

Eggshell is a natural bio-ceramic composite with a unique chemical composition consist of high inorganic content (~95% of calcium carbonate) and ~4% of organic components.[8–10] The mechanical properties of eggshells are influenced by the interaction between these organic and inorganic constituents.[11] The distinctive structure of eggshell combined with the substantial availability makes eggshell a potential source of bio-fillers that can be efficiently used for polymer nanocomposites. Researchers have reported the use of eggshells as a reinforcement material in polymer matrices. Toro et al. used different weight fractions of chicken eggshell as bio-filler to improve the properties of polypropylene. The average size of the eggshell particles was ~8.4 μm and the surface area was ~18 m^2/g. The mechanical properties of eggshell/polypropylene composite showed significant improvements compared to other polypropylene composites reinforced with commercial talc and calcium carbonate fillers. Moreover, eggshell/polypropylene composites

demonstrated better eggshell/matrix interface. The formed polypropylene composite[12] contained eggshell reinforcements with weight fractions varied from 20 to 60%. Arias et al. developed eggshell/polypropylene composites with improved mechanical and thermal properties compared with polypropylene composite reinforced by traditional mineral particles.[13] Ji et al. also reported substantial improvements in the mechanical performance of diglycidylether bisphenol A epoxy resin infused with 5 wt % of chicken eggshell microparticles (average particles size 9.36 μm and 17.4 m^2/g surface area).[14] Xu and Hanna studied the infusion of 2, 6, and 10% by weight of eggshell particles in a composite foam material derived from corn starch for food packaging application. The as-prepared composites exhibited enhanced thermal and mechanical properties due to the infusion of micron size eggshell particles.[15] It is evident from the literature that all the studies describe the incorporation of micron size calcium carbonate particles derived from eggshells in polymeric composites as reinforcements.[3,12–15] It is also worth mentioning that the particle loading in these studies are very high. The aim of this study is to investigate the effect of small loading (1, 2, and 3% by weight) of nano-size bio-calcium carbonate particles in bio-based thermoset resin on the thermal and mechanical properties of composites.

The dispersion of additives and fillers in the polymer matrix is one of the important aspects of polymer processing. The degree with which the nanoparticles can be homogeneously dispersed in the polymer matrix would significantly influence the thermal and mechanical properties of the material. Poor dispersion can lead to a diminution of the properties in the resulting material. Researchers have reported a number of nanoparticles dispersion methods including (1) mechanical agitation, such as ball milling or magnetic stirring, (2) ultrasonic vibration, (3) shear mixing, (4) noncontact mixing, and (5) using a dispersing agent. In this investigation we have used the noncontact mixing method. Noncontact mixing is one of the proven techniques for effective mixing of polymers, powders and fillers. In this technique the material container is set at 45° angle inside the mixer and revolves and rotates at high acceleration with the speed of ~2000 rpm. Dual centrifugal forces were given to the container that keep pressing materials to down and outward along with the slope of the inner wall of the container and accomplish powerful mixing and deaerating simultaneously. This technique is noncontact and nonreactive unlike ultrasound and other mixing techniques. One of the major advantages of this mixing technique is the considerable reduction of processing time.[16–19] We have used this method in our previous study to fabricate WO_3/SC-15 epoxy nanocomposites, and the TEM results showed that the particles were well dispersed over the entire volume of the epoxy resin.[20] Hoa et al. prepared carbon nanofibers-based composites using a method combining ultrasonication and mechanical mixing. The mixture was mixed under vacuum with a Thinky mixer at 2000 rpm, and the results showed that good dispersion was achieved due to the use of this mixing method.[21] Chika Taka et al. have also used this mixing technology to synthesize high solid content yttria slurry, and their SEM observation confirmed that the slurry was well dispersed.[22] Thinky mixing represents an efficient mixing and dispersion technique.[23–26]

In this investigation, we have used a noncontact mixing technique for dispersion of bio-calcium carbonate nanoparticles synthesized from eggshells in Polylite 31325 bio-based resin polymer. In parallel, a control panel was also fabricated from the neat Polylite resin to compare the enhancement or degradation of the thermal and mechanical properties due to bio-calcium carbonate nanoparticles reinforcement.

EXPERIMENTAL

Materials

The materials used in this study are bio-inspired materials that are obtained from renewable resources. Eggshells were used as raw material for the synthesis of bio-$CaCO_3$ nanoparticles that was used as reinforcement nanofillers. Commercially available Polylite® 31325-00 thermoset resin was used as polymeric matrix. This polymer is a nonpromoted, medium reactive, low viscosity unsaturated polyester molding resin that is based on soybean oil resin and has a green content of ~25%. Polylite® 31325-00 resin was provided by Reichhold, USA, Research Triangle Park, NC. Methyl ethyl ketone peroxide (MEKP) and cobalt naphthanate with 6% metal content (CoNap) were used as the initiator and accelerator respectively in the fabrication of neat Polylite and the bio-nanocomposite systems. Chemicals used in this study were purchased from Sigma-Aldrich, St. Louis, MO.

Fabrication of Bio-$CaCO_3$/Polylite 31325 Bio-Nanocomposites

In this study the $CaCO_3$ nanoparticles used were derived from chicken eggshells. Bio-calcium carbonate nanoparticles have been synthesized via a top-down approach for producing nanostructured materials. The process started with cleaning and drying of eggshells. After that, the shells were ground with a coffee grinder to produce eggshells fine powder. The powder has been further subjected to a size reduction process using the mechanical attrition method. In this method, the eggshell powder was ball milled using a high energy SPEX SamplePrep 8000D Dual Mixer/Mill for 10 h in the presence of polypropylene glycol as a medium. These particle sizes were standardized by passing through a standard mesh using a high speed shaker. The particles were separated by a set of standard stainless steel sieves 95 and 20 μm in size. Further size reduction was carried out to achieve nano sized particles using the sonochemical method.[27] During this step eggshell particles were irradiated with a high intensity ultrasonic horn (Ti-horn, 20 kHz, and 100W/cm^2) in the presence of dimethylformamide (DMF) for 5 h.

Three different loadings of bio-calcium carbonate nanoparticles were used with Polylite 31325 resin, including 1, 2, and 3% loadings by weight to fabricate bio-$CaCO_3$/Polylite 31325 bio-nanocomposite samples at a 100 g basis. In the first step of the fabrication process, known percentage of bio-$CaCO_3$ nanoparticles and Polylite resin were added to the mixing container and mixed using a noncontact THINKY hybrid defoaming mixer *ARE-250* for 10 min to completely disperse the particles in the resin and result in a uniform mixture without any air bubbles in a relatively short time.[20] In the next step, 380 μL of cobalt naphthanate with 6% metal content (CoNap) (equivalent to 0.6 g) was added to the mixture, and all the materials were mixed again for another 10 min using the THINKY mixer. After

that, 960 μL of methyl ethyle ketone peroxide (MEKP) was added to the container contents and mixed for another 3 min. CoNap (accelerator) and MEKP (initiator) were added to the mixture on volume basis using an adjustable micropipette for more accurate measurements. These quantities of CoNap and MEKP allowed for ~5 min before the resin started to gel and solidify. Finally, the nanoparticles/resin mixtures were poured into a steel container and cured at 65°C for 24 h and then post cured at 125°C for 4 h in a conventional oven. This procedure was repeated for three different weight percentages of the bio-$CaCO_3$ nanoparticles (1, 2, and 3 wt %) to make the bio-nanocomposites. A neat control sample of Polylite 31325 resin was also fabricated using the same procedure without adding bio-$CaCO_3$ nanoparticles for comparison purpose. The samples were cut precisely and used for thermal and mechanical testing.

Characterization

X-ray diffraction measurements were conducted using a Rigaku D/MAX 2200 X-Ray diffractometer to investigate the crystal structure of bio-$CaCO_3$ nanoparticles. These measurements were also used to study the exfoliation of bio-$CaCO_3$ in as-prepared bio-nanocomposites. The XRD samples were prepared by uniformly spreading the bio-$CaCO_3$ nanoparticles on quartz sample holder, whereas the as-prepared neat polymers and bio-nanocomposites cured samples were cut precisely and mounted in an aluminum sample holder. XRD tests were conducted at room temperature from 10° to 80° of 2θ. The pattern peaks resulting from the diffraction were analyzed using the Jade 9 software.

High resolution transmission electron microscopy (HRTEM) has been performed on as-prepared bio-$CaCO_3$ nanoparticles and 2 wt % bio-$CaCO_3$ nanoparticles infused Polylite 31325 resin, using JOEL-2010 transmission electron microscope. TEM samples were prepared by dispersion of nanoparticles in ethanol using a sonication bath for 5 min at room temperature and a drop of solution was placed on a copper grid (carbon coated copper grid-200 mesh) then dried in air and used for TEM analysis. The 2% bio-$CaCO_3$ nanoparticles infused Polylite 31325 bio-nanocomposites samples were prepared using a Leica EM UC6 microtome.

To obtain information about the thermal stability of the neat polymer and nanocomposite systems synthesized in this study, TGA of as-prepared neat and bio-nanocomposite samples were carried out under nitrogen gas atmosphere on a Mettler Toledo TGA/SDTA 851e apparatus. The samples were precisely cut into small pieces (~10–20 mg) and kept in an aluminum oxide sample pan. The TGA measurements were carried out from 30°C to 800°C at a heating rate of 10°C/min. Real time characteristic curves were generated by a Mettler data acquisition system. These analyses were carried out using ASTM Standard E1131-03.

DSC experiments were also carried out using a Mettler Toledo DSC 822^e. DSC experiments were conducted from room temperature to 500°C at a heating rate of 10°C/minute under nitrogen gas atmosphere. The samples were precisely cut into small pieces of 10–20 mg, kept in an aluminum sample pan and used for DSC analysis. These tests were carried out using ASTM Standard E1356-03.

Thermo mechanical analysis (TMA) experiments of neat polymers and bio-$CaCO_3$ reinforced polymer nanocomposites were carried out on a TA Instruments thermomechanical analyzer TMA Q400. The samples were cut into small pieces of dimensions 5 mm x 5 mm x 5 mm using a diamond cutter and machined using a mechanical grinder to maintain the specified sample dimensions according to standard ASTM E 831-06. Dimensional changes were measured in the thickness direction and the temperature was ramped from room temperature to 180°C. Dynamic mechanical analysis DMA of various specimens was carried out on a TA Instruments dynamic mechanical analyzer DMA Q800. The samples were cut into small pieces using a diamond cutter and machined using a mechanical grinder to maintain the specified sample dimensions. The width of the samples was 12 mm and span length to thickness ratio was 10. The test was carried out according to ASTM D4065-01. The tests were run on a double cantilever beam mode with a frequency of 1 Hz and amplitude of 15 μm. The temperature was ramped from room temperature to 180°C and the heating rate was maintained at 5°C/min throughout the test runs so that there was a minimum temperature lag between the sample and the furnace environment. From the test data, storage modulus, loss modulus, and tan delta were determined.

Flexural tests under three-point bend (TPB) configuration were performed according to ASTM D790-02. Test specimens length and width are 100 and 13 mm, respectively. The span length is 80 mm and average sample thickness is 4.8 mm. The tests were conducted in a 2.5 kN Zwick Roell Z 2.5 testing machine equipped with TestXpert data-acquisition system. The machine was operated under displacement control mode at a crosshead speed of 2.0 mm/min, and all the tests were performed at room temperature. Stress–strain data for each sample was collected. Flexural strength and modulus were calculated from the slope of the stress Vs strain plot. Five samples were tested from each material and the average values of flexural strength and modulus were determined.

To investigate the quasi-static compression response of neat Polylite 31325 and bio-$CaCO_3$/Polylite 31325 nanocomposite systems, quasi-static compression tests were performed. The specimens were tested in the thickness direction using servo-hydraulically controlled material testing system (MTS-810) with 100 KN capacity. ASTM C365–57 standard was followed for the quasi-static compression test. The size of test specimens was 12.7 mm in diameter and 25.4 mm in thickness. The test was carried out at room temperature in displacement control mode and the crosshead speed was 1.27 mm/s. To maintain evenly distributed compressive loading, each test specimen was sanded and polished with high accuracy to ensure that the opposite faces were parallel to one another. A total of five specimens of each type of material were tested. A software Test Ware-SX was used to develop a program which controlled the test conditions and recorded both the load and crosshead displacement data. The load-deflection data recorded by the data acquisition system was converted to stress–strain curves and used in the calculations of the compressive strength and modulus.

Scanning electron microscopy (SEM) analysis was carried out using a JEOL JSM 5800 scanning electron microscope to study the fracture surface of samples in response to flexural load at the microscopic level. The failed samples of neat Polylite 31325 resin and bio-$CaCO_3$/Polylite nanocomposites were cut into small pieces and placed on a double-sided adhesive conductive carbon tape and coated with a thin layer of gold/palladium mixture (Au/Pd) using a sputter coater Hummer 6.2 to prevent charge buildup by the electron absorption by the specimen.

RESULTS AND DISCUSSION

To investigate the crystal structure and impurities presented in the bio-$CaCO_3$ nanoparticles derived from eggshells, XRD analysis was conducted. The XRD pattern of bio-$CaCO_3$ nanoparticles is presented in Figure 1(a) and all the peaks matched very well that of calcium carbonate $CaCO_3$ in the form of calcite (JCPDS card No. 47-1743). These results clearly indicate the high purity of inorganic calcium carbonate in the bio-inspired nanoparticles and no impurities were observed. The XRD patterns of neat Polylite 31325 resin and bio-$CaCO_3$/Polylite 31325 nanocomposites are also presented in Figure 1. The characteristic peaks in XRD patterns of Figure 1(a–e) match with the $CaCO_3$ JCPDS card No. 47-1743. The XRD curve for neat Polylite resin show a distinctive wide peak at $\sim 18^\circ$ of 2θ as seen in Figure 1(b), this peak is assigned to the polymer. A comparison of the intensities of the characteristic $CaCO_3$ peaks between the XRD pattern of bio-$CaCO_3$ nanoparticles and the XRD patterns for the as-prepared nanocomposites show a decrease in the peak intensities of all the as-prepared nanocomposites suggesting that the bio-$CaCO_3$ nanoparticles are highly exfoliated in the polymer matrix due to the good dispersion attained by the non-contact mixing technique used in the fabrication process.[20]

TEM was used to determine the shape and size of as-prepared bio-$CaCO_3$ nanoparticles. Figure 2(a) represents a TEM micrograph of bio-$CaCO_3$ nanoparticles. As seen in the image all the nanoparticles are uniform and below 10 nm in size; moreover, they demonstrate highly crystalline structure and irregular shapes that influence and increase the surface area of these nanoparticles.

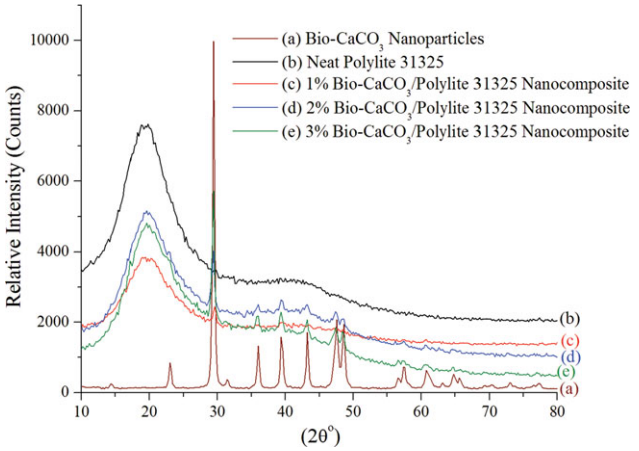

Figure 1. XRD patterns of bio-$CaCO_3$ nanoparticles, as-prepared neat Polylite 31325 and bio-$CaCO_3$/Polylite 31325 nanocomposites. [Color figure can be viewed in the online issue, which is available at wileyonlinelibrary.com.]

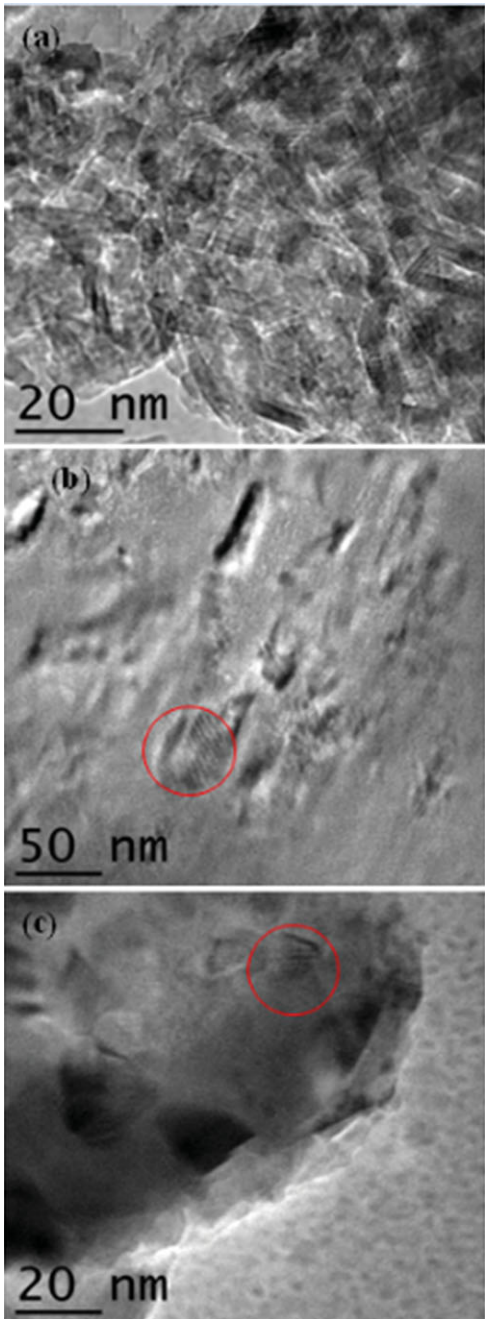

Figure 2. TEM micrographs of (a) bio-$CaCO_3$/nanoparticles, (b, c) 2% bio-$CaCO_3$/Polylite 31325 nanocomposite. [Color figure can be viewed in the online issue, which is available at wileyonlinelibrary.com.]

TEM was also used to investigate the dispersion of bio-$CaCO_3$ nanoparticles in Polylite 31325 resin. Figures 2(b,c) represent the TEM micrographs of the 2% bio-$CaCO_3$/Polylite 31325 nanocomposite and clearly show that the as-prepared bio-$CaCO_3$ nanoparticles are very well dispersed over the entire volume of the matrix even at a relatively high magnification of

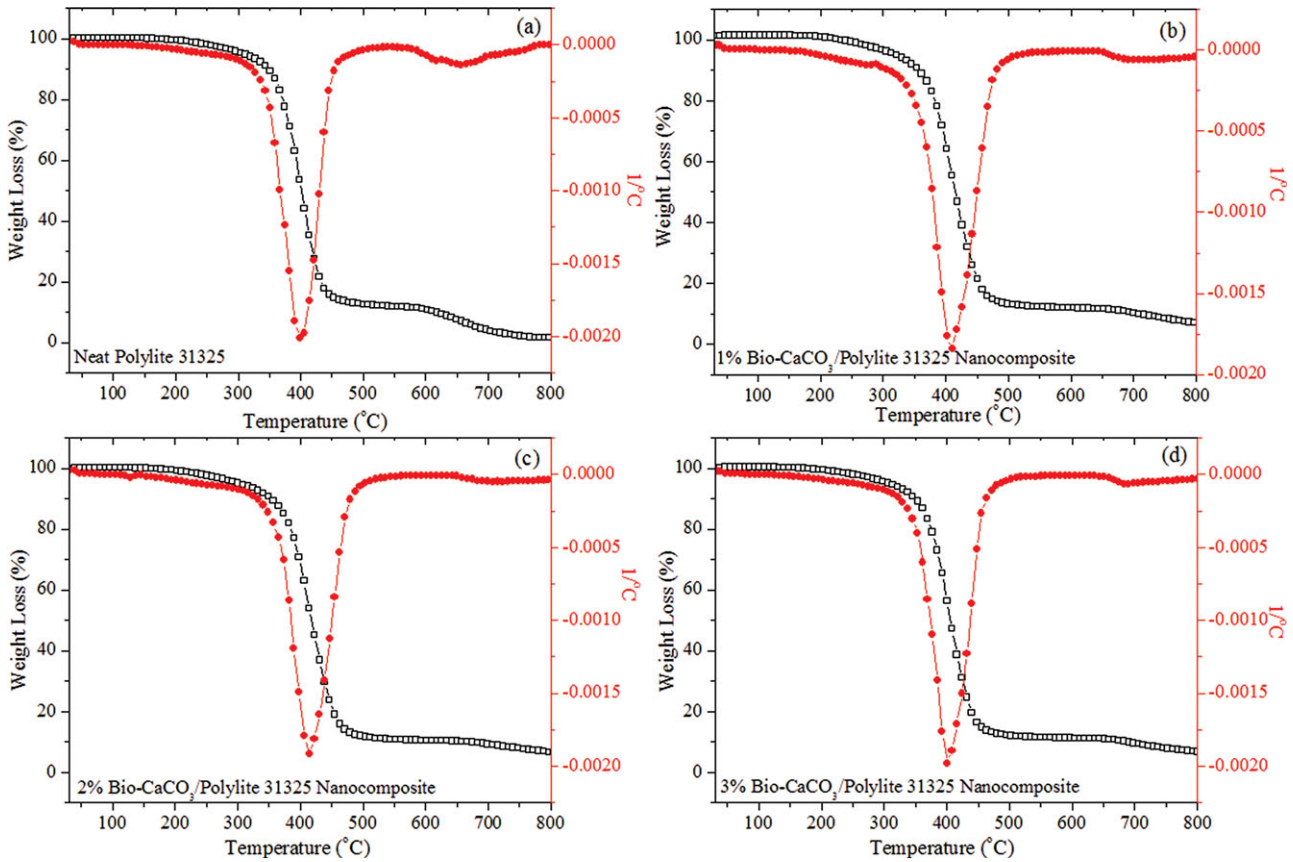

Figure 3. TGA results for (a) neat Polylite 31325 and (b, c and d) 1, 2, and 3% bio-$CaCO_3$/Polylite 31325 nanocomposite. [Color figure can be viewed in the online issue, which is available at wileyonlinelibrary.com.]

~50 nm scale. We have conducted the TEM analysis for only 2 wt% of Bio-$CaCO_3$ nanoparticles infused Polylite 31325 resin because it was the system that showed the best thermal and mechanical improvements. In Figure 2(c), the micrograph, taken at a higher magnification (~20 nm scale) also illustrates the good dispersion of the nanoparticles in Polylite 31325, and both of the TEM micrographs show the highly crystalline bio-$CaCO_3$ nanoparticles with very distinguished lattice planes.

Thermogravimetric analysis (TGA) measurements were carried out to obtain information on the thermal stability of neat Polylite 31325 and bio-$CaCO_3$/Polylite 31325 nanocomposites. In the present TGA studies, the peak of the derivative curve was considered as a marker for structural decomposition of the samples.[28,29] Figures 3(a–d) depict the TGA graphs of neat Polylite 31325 and 1, 2, and 3% bio-$CaCO_3$/Polylite 31325 nanocomposite, respectively. As seen in the Figure, the major structural disintegration for neat Polylite 31325 resin occurs at ~400°C, while it takes place at 408.4°C for 1% bio-$CaCO_3$/Polylite 31325 nanocomposite. The neat Polylite 31325 sample also exhibit a second weight loss at ~650°C; this weight loss is delayed by ~20°C degrees (~670°C) for 1% bio-$CaCO_3$/Polylite 31325 nanocomposite. As seen in Figure 3(c), the major structural disintegration for 2% bio-$CaCO_3$/Polylite 31325 nanocomposite occurs at 415°C, while for 3% bio-$CaCO_3$/Polylite 31325 nanocomposite it occurs at 402°C as presented in Figure 3(d). All of these samples also exhibit second weight loss at higher temperatures (~680°C); this weight loss temperature has increased by ~30°C in nanophased Polylite 31325 compared with the neat Polylite 31325 resin. The decomposition temperature for 1, 2, and 3% bio-$CaCO_3$/Polylite 31325 nanocomposite has increased by 8, 15, and 8°C, respectively compared with the neat Ploylite 31325 resin suggesting better thermal stability of the as-prepared nanocomposites.

One of the most important factors that strongly affects the thermal stability of thermosetting polymers is the extent of crosslinking; the higher the density of the crosslinks, the higher the thermal stability or the allowable use temperature.[30] The increase in thermal stability of nanophased Polylite 31325 is due to the catalytic effect on the crosslinking of the polymer caused by the reactive high surface area bio-$CaCO_3$ nanoparticles. These results are also consistent with the comparison of 50% weight loss temperatures. TGA results of neat Polylite 31325 and bio-$CaCO_3$/Polylite 31325 nanocomposites are summarized in Table I. It is clear from the TGA results that the as-prepared bio-nanocomposite sample containing 2% by weight of bio-$CaCO_3$ nanoparticles have the highest decomposition temperature and are thermally more stable than all other samples.

DSC curves of neat and nanophased Polylite 31325 resin samples are shown in Figure 4 and the results are summarized in Table I. The glass transition temperatures (T_g) of the samples

Table I. TGA and DSC Results for Neat Polylite 31325 and Bio-$CaCO_3$/Polylite 31325 Nanocomposites

	Sample	Decomposition temperature T_d (°C)	Degrees increased (°C)	50% weight loss temperature (°C)	Degrees increased (°C)	Glass transition temperature T_g (°C)	Degrees increased
1.	Neat Polylite	400.3 ± 2.2	-	402 ± 1.3	-	108 ± 1	-
2.	1% Bio $CaCO_3$/Polylite	408.4 ± 1.8	8.1	412 ± 2.4	10	117 ± 1	9
3.	2% Bio-$CaCO_3$/Polylite	415.2 ± 3.0	14.9	420 ± 2.9	18	126 ± 2	18
4.	3% Bio-$CaCO_3$/Polylite	402.6 ± 2.1	2.3	408 ± 1.9	6	113 ± 1	5

were obtained from the DSC curves as the inflection points of the heat flow curves.[31,32] The T_g of the neat Polylite 31325 resin is detected as the broad change in baseline at 108°C. The T_gs measured for 1, 2, and 3% bio-$CaCO_3$/Polylite 31325 nanocomposite are 117°C, 126°C, and 113°C, respectively.

These DSC results show that the T_gs have increased by 9°C for 1%, 18°C for 2% and 5°C for 3% bio-$CaCO_3$/Polylite 31325 nanocomposites systems compared to the neat Polylite 31325. This increase in T_g is explained as the increase in the cross-linking of the resin in the presence of bio-$CaCO_3$ nanoparticles. The glass transition temperature of the resin is closely related to the cross linking degree of resin: the higher the cross linking, the higher the T_g. Usually T_g increases with increasing cross-linking density of resins because of the restriction in molecular chain mobility imposed by cross-linking.[33,34] This effect can be understood in terms of decreasing free volume.[35] The exothermic peaks in the DSC curves at high temperature in the range of 400–450°C are related to the decomposition of the polymer, and these results are comparable with the TGA results.

Thermo mechanical analysis (TMA) measurements were carried out to obtain information on the dimensional stability of the as-prepared bio-nanocomposites under variation of temperature. Figure 5 depicts the dimensional change in one direction for neat Polylite 31325 resin and bio-$CaCO_3$/Polylite 31325 nanocomposites as a function of temperature. As seen in Figure 5, the dimensional changes for all samples occur non-linearly up to the glass-transition region where phase-transformation occurs. Beyond the glass-transition temperature, the variations of dimensional change are fairly linear. The calculated co-efficient of thermal expansion (CTE) are shown in Table II. As seen in Table II, the CTEs below and above T_g for bio-$CaCO_3$/Polylite 31325 nanocomposites have reduced significantly compared to the neat Polylite 31325 resin.

The improvement in the thermal stability for bio-$CaCO_3$/Polylite 31325 nanocomposites is due to the incorporation of highly exfoliated bio-$CaCO_3$ nanoparticles. In the as-prepared bio-nanocomposite; the bio-$CaCO_3$ nanoparticles contribute in reducing the molecule movement upon heating. As the temperature increases, the well dispersed nanoparticles neither deform nor relax like the resin molecules. The rigid bio-$CaCO_3$ nanoparticles effectively retard the thermal expansion of the resin molecules causing the CTEs both below and above T_g of bio-$CaCO_3$/Polylite 31325 nanocomposites to be lower than the CTE of the neat Polylite 31325 resin.

The dynamic mechanical analysis reveals the amount of energy stored in the nanocomposite as elastic energy and the amount of energy dissipated during mechanical strain, which strongly depends on the geometrical characteristic and the level of

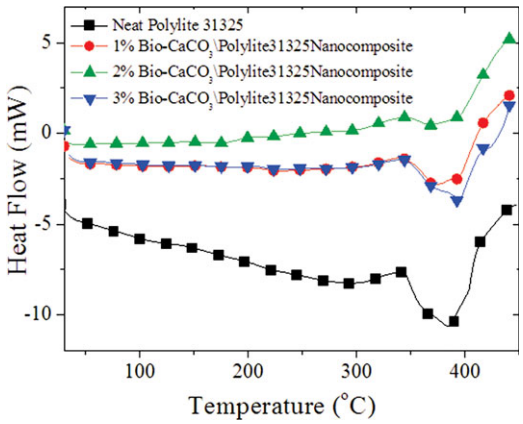

Figure 4. DSC results for neat Polylite 31325 and bio-$CaCO_3$/Polylite 31325 nanocomposites. [Color figure can be viewed in the online issue, which is available at wileyonlinelibrary.com.]

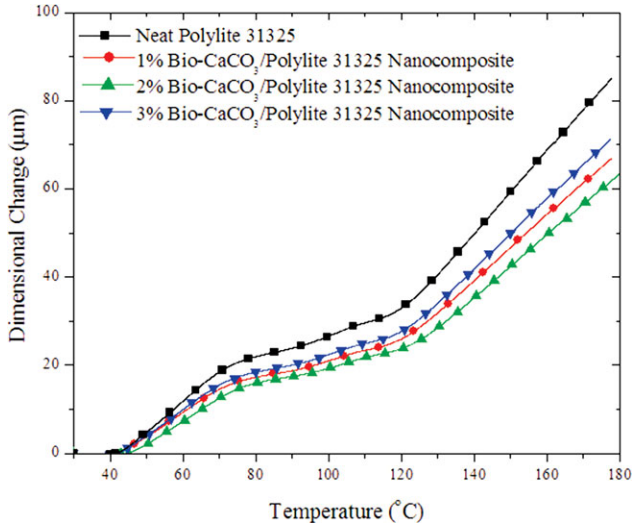

Figure 5. Dimensional change vs. temperature plot for neat Polylite 31325 resin. [Color figure can be viewed in the online issue, which is available at wileyonlinelibrary.com.]

Table II. CTE Results for Neat Polylite 31325 and Bio-$CaCO_3$/Polylite 31325 Nanocomposites

No.	Sample	CTE (μm/m°C) Below T_g (50–70°C)	CTE (μm/m°C) Above T_g (150–170°C)
1.	Neat Polylite	82.8 ± 1.4	187.9 ± 2.1
2.	1% Bio-$CaCO_3$/Polylite	64.3 ± 2.2	144.2 ± 1.7
3.	2% Bio-$CaCO_3$/Polylite	63.2 ± 1.8	142.8 ± 1.2
4.	3% Bio-$CaCO_3$/Polylite	68.6 ± 1.0	154.7 ± 2.4

dispersion of the reinforcing fillers in the matrix. It also depends on the degree of interaction between the matrix and filler surface.[36] Storage modulus, loss modulus and the phase lag (tan δ) for neat and nanophased polymers were determined from DMA studies. Storage modulus for neat Polylite 31325 and bio-$CaCO_3$/ Polylite 31325 nanocomposites are presented in Figure 6, and the results are shown in Table III. At room temperature the storage moduli of all bio-$CaCO_3$/Polylite 31325 nanocomposites are found to be higher than that of the neat Polylite 31325 nanocomposites and are promoted as bio-$CaCO_3$ nanoparticles loading increased from 1% to 2% and then dropped for the 3% bio-$CaCO_3$/ Polylite 31325 nanocomposites. When the temperature increased to 100°C, the storage modulus for 2% bio-$CaCO_3$/Polylite 31325 nanocomposites was increased to 711 MPa as compared to neat Polylite 31325 (439.6 MPa), 1% bio-$CaCO_3$/Polylite 31325 nanocomposite (521.9 MPa) and 3% bio-$CaCO_3$/Polylite 31325 nanocomposite (509.3 MPa). This increase may be assigned to the strong interfacial interaction between the resin system and the bio-$CaCO_3$ nanoparticles as reinforcement sites.

Loss modulus results for neat Polylite 31325 and bio-$CaCO_3$/ Polylite 31325 nanocomposites are presented in Figure 7 and listed in Table III. The room temperature value for the loss modulus of 1% bio-$CaCO_3$/Polylite 31325 nanocomposite is found to be higher than that of the neat Polylite 31325 and other bio-$CaCO_3$/Polylite 31325 nanocomposites. For neat Polylite 31325, the loss modulus is 123.7 MPa, while for 1%, 2% and 3% bio-$CaCO_3$/Polylite 31325 nanocomposites, the loss moduli are 198.6 MPa, 154.5 MPa and 112.9 MPa, respectively. At 140°C, an improvement in the loss modulus was noticed for all nanophased samples as compared to neat Polylite 31325. For neat Polylite 31325, the loss modulus is 16.3 MPa, while for 1%, 2% and 3% bio-$CaCO_3$/Polylite 31325 nanocomposites, the loss moduli are 18.8 MPa, 26.9 MPa and 17.1 MPa respectively. Loss modulus for neat and nanophased Polylite 31325 decreased to lower values tending to 1 MPa when the temperature was raised to higher degrees as seen in the Table III. Bio-$CaCO_3$/Polylite 31325 Nanocomposite exhibited improvements in glass transition temperatures measured by DMA for the evaluation of the maximum peaks of Tan (δ) curves as shown in Figure 8 and Table III. T_g for neat Polylite 31325 resin measured by this technique was found to be 126.8°C, whereas for 1, 2, and 3% bio-$CaCO_3$/Polylite 31325 nanocomposites, the T_gs were 127.4°C, 131.7°C and 130.1°C, respectively. This increase in the glass transition temperature is attributed to the increase in the cross-linking of the polymer due to the uniform dispersion of bio-$CaCO_3$ nanoparticles. To further confirm we have calculated the cross link density using the equation reported in the literature.[37]

$$E_r = 3RT_r\, v_e$$

In this equation the rubbery modulus, E_r shown in Table III is taken as the storage modulus at 30°C above the glass

Table III. (a) DMA Storage Modulus and Crosslinking Density of Neat Polylite 31325 and Bio-$CaCO_3$/Polylite 31325 Nanocomposites; (b) DMA Loss Modulus Results of Neat Polylite 31325 and Bio-$CaCO_3$/Polylite 31325 Nanocomposites

No	Sample (a)	Storage modulus, E' (MPa) At 30°C	Storage modulus, E' (MPa) At 140°C	Cross link density Mol/m^3
1.	Neat Polylite	1751 ± 64	68.9 ± 12	6688
2.	1% Bio-$CaCO_3$/Polylite	2209 ± 58	80.6 ± 9	7824
3.	2% Bio-$CaCO_3$/Polylite	2421 ± 78	94.2 ± 17	9145
4.	3% Bio-$CaCO_3$/Polylite	1846 ± 55	63.5 ± 21	6164
		Loss modulus, E″ (MPa)		
No	Sample (b)	At 30°C	At 140°C	T_g°C
1.	Neat Polylite	123.7 ± 6.1	16.3 ± 5.1	126.8 ± 1.6
2.	1% Bio-$CaCO_3$/Polylite	198.6 ± 4.7	18.8 ± 4.1	127.4 ± 2.1
3.	2% Bio-$CaCO_3$/Polylite	154.5 ± 4.2	26.9 ± 3.6	131.7 ± 1.2
4.	3% Bio-$CaCO_3$/Polylite	112.9 ± 3.9	17.1 ± 4.2	130.1 ± 0.8

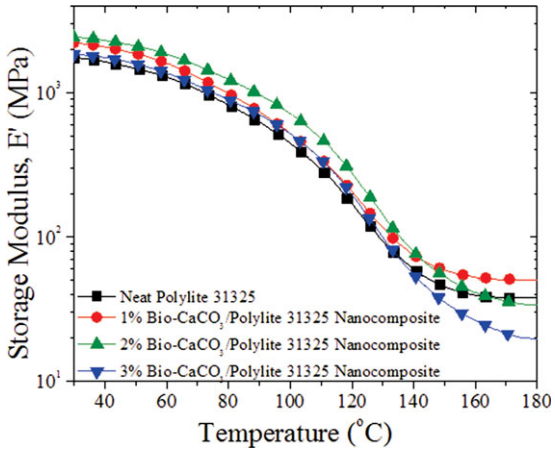

Figure 6. Storage Modulus for neat Polylite 31325 and bio-$CaCO_3$/Polylite 31325 nanocomposites. [Color figure can be viewed in the online issue, which is available at wileyonlinelibrary.com.]

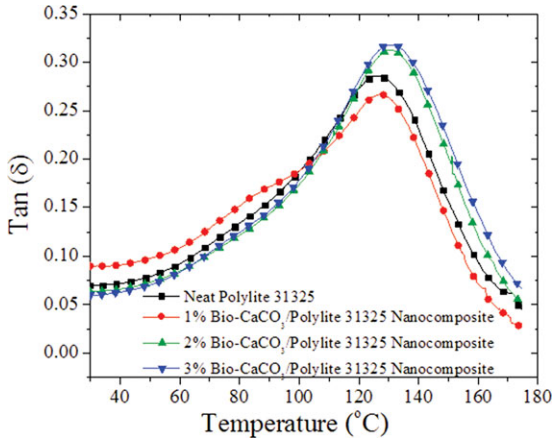

Figure 8. Tan (δ) results for neat Polylite 31325 and bio-$CaCO_3$/Polylite 31325 nanocomposites. [Color figure can be viewed in the online issue, which is available at wileyonlinelibrary.com.]

temperature[38]. 2wt% bio-$CaCO_3$/Polylite 31325 nanocomposites has higher E_r than neat Polylite 31325, 1 and 3 wt % of bio-$CaCO_3$/Polylite 31325 nanocomposites, which indicates that the 2 wt % bio-$CaCO_3$/Polylite 31325 nanocomposites has the increased crosslink density. To be quantitative, we have also estimated the crosslink density from the above equation. Where R is the universal gas constant, T_r is the temperature corresponding to E_r, and v_e is the crosslink density. As shown in Table III, the crosslink density increase from 6688 mol/m^3 to 9145 mol/m^3 for neat to 2wt% loading of bio-$CaCO_3$ nanoparticles. These results are consistent with the TGA and DSC results. Although there is a significant increase in the T_g for nanophased Polylite 31325 resin compared to the neat Polylite 31325 resin, these values of T_gs are much higher than the T_g values determined by DSC. These differences are associated with the differences in the testing techniques between DSC and DMA. In DMA the damping peak is associated with the loosening of the polymer structure so that group and small chain segments can move, and this occurs near T_g at low frequencies. The Tan (δ) peak at frequency of 1 Hz generally is at temperature 15–20 degrees above the T_g value measured by DSC. This is commonly observed in polymeric systems and is very well documented.[39–42]

The mechanical performance of polymeric nanocomposite material depends on the dispersion of nanoparticles and interfacial interaction between nanoparticles and the polymer matrix. Flexural tests were performed to determine the flexural strength and modulus of as-fabricated neat polymers and bio-nanocomposites. Typical stress-strain curves from the flexural tests for neat Polylite 31325 and bio-$CaCO_3$/Polylite 31325 bio-nanocomposites are shown in Figure 9 and a summary of the results is presented in Table IV. All values were based on an average of 5 tested specimens and the results are presented in Figure 9 inset as bar graph with error bars. As seen in Figure 9, the

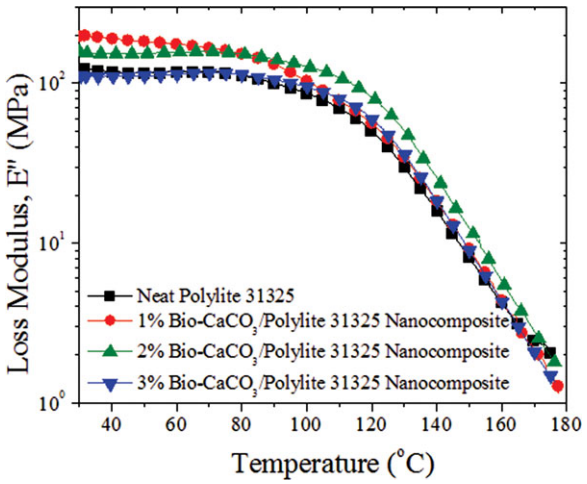

Figure 7. Loss Modulus for neat Polylite 31325 and bio-$CaCO_3$/Polylite 31325 nanocomposite. [Color figure can be viewed in the online issue, which is available at wileyonlinelibrary.com.]

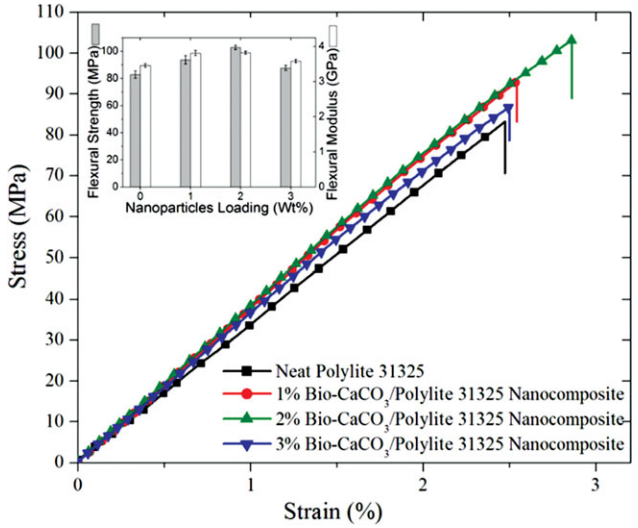

Figure 9. Stress–strain curve of flexure test results for neat Polylite 31325and bio-$CaCO_3$/ Polylite 31325 nanocomposites. Inset is a bar graph of flexural results with error bars. [Color figure can be viewed in the online issue, which is available at wileyonlinelibrary.com.]

Table IV. Flexure Tests Results for Neat Polylite 31325 and Bio-$CaCO_3$/Polylite 31325 Nanocomposites

No.	Sample	Flexural strength (MPa)	Increase (%)	Flexural modulus (GPa)	Increase (%)
1.	Neat Polylite	82.8 ± 2.7	-	3.456 ± 0.051	-
2.	1% Bio-$CaCO_3$/Polylite	93.6 ± 3.1	13.0	3.811 ± 0.074	10.3
3.	2% Bio-$CaCO_3$/Polylite	102.8 ± 1.7	24.2	3.823 ± 0.043	10.6
4.	3% Bio-$CaCO_3$/Polylite	87.7 ± 1.9	5.9	3.583 ± 0.049	3.7

stress-strain behavior for neat Polylite 31325 and 1%, 2% and 3% bio-$CaCO_3$/Polylite 31325 nanocomposites is linear up to the failure point. The inclusion of bio-$CaCO_3$ nanoparticles have increased the flexure strength for all bio-nanocomposite samples compared to the neat resin. The flexure strength of neat Polylite 31325 resin is 82.8 MPa. The flexure strength has increased by 13% for 1% bio-$CaCO_3$/Polylite 31325 nanocomposite (93.6 MPa). It has also increased substantially for 2% bio-$CaCO_3$/Polylite 31325 nanocomposite by 24.2% to reach 102.8 MPa and by 5.9% for 3% bio-$CaCO_3$/Polylite 31325 nanocomposite (87.7 MPa). A similar trend of improvements was observed for the flexure modulus as well. The flexure modulus of neat Polylite 31325 resin is 3.456 GPa while it is 3.811 GPa for 1% bio-$CaCO_3$/Polylite 31325 nanocomposites with a 10.3% increase. Other loadings of bio-$CaCO_3$ nanoparticles in the resin have caused an increase in the flexure modulus as well, compared to the neat Polylite 31325 nanocomposites. The flexure moduli of 2% and 3% bio-$CaCO_3$/Polylite 31325 nanocomposites are 3.822 GPa (10.6% increase) and 3.583 GPa (3.7% increase), respectively.

The increase of flexure strength and modulus in the bio-nanocomposite systems is due to the presence of nano sized bio-$CaCO_3$ nanoparticles which have high surface area that improve the cross-linking of the polymer and subsequently enhance the mechanical and thermal properties, helping the bio-nanocomposites to withstand higher loads. Another reason for the increase in the flexural properties is the degree of dispersion of bio-$CaCO_3$ nanoparticles in the Polylite 31325 resin. Excellent dispersion was very much evident by the XRD and TEM results.[43] It is worth mentioning that surprisingly the strain-to-failure is also increased as compared to the neat Polylite 31325. The reason for increasing the strain to failure may be due to the presence of highly porous bio-$CaCO_3$ nanoparticles.

To further understand the mechanical behavior of bio-$CaCO_3$/Polylite 31325 nanocomposites, quasi-static compression tests were carried out for five samples of each neat Polylite 31325 and bio-$CaCO_3$/Polylite 31325 nanocomposites. All values were based on an average of 5 tested specimens and the results are presented in Figure 10 inset as bar graph with error bars. Stress–strain curves of 1%, 2% and 3% bio-$CaCO_3$/Polylite 31325 nanocomposites, along with neat Polylite 31325 resin are shown in Figure 10, and the results are summarized in Table V. It is observed from Figure 10 that the compressive strength and modulus of 2% bio-$CaCO_3$/Polylite 31325 nanocomposite are 91.8 MPa and 2618 MPa, respectively. However the neat Polylite 31325 resin compressive strength and modulus are 80.3 MPa and 2061.4 MPa, respectively. These results show a 14% increase in strength and 27% increase in modulus as compared to the neat Polylite 31325 resin system. The 2% loading of bio-$CaCO_3$ nanoparticles show the highest mechanical properties among the 1% and 3% loading of bio-$CaCO_3$ nanoparticles. The compressive properties for 1% and 3% loadings of bio-$CaCO_3$ nanoparticles are lower compared to the 2% loading of bio-$CaCO_3$ nanoparticles, but they are still higher than the compressive properties for neat Polylite 31325 thermosetting polymer. The reason for this can be explained as for the 1% bio-$CaCO_3$/Polylite 31325 nanocomposite, the amount of bio-nanoparticles is not sufficient to achieve the maximum enhancement of the mechanical properties. For 3% bio-$CaCO_3$/Polylite 31325 nanocomposite, the increase in the loading of bio-nanoparticle in the resulting bio-nanocomposites will begin to experience more and more particle-to-particle interaction rather than the intended particle-to-polymer interaction. Particle-to-particle interaction will lead to particle agglomerations and poor mechanical properties. These mechanical properties are consistent with the thermal and microscopic properties. Figure 10 also contains a stress plateau region that indicates that these bio-nanocomposites have an ability to absorb compressive damage. The plateau also occurs in the case of the neat system but at lower compression loads. These curves are similar to those observed by other researchers.[44]

The fracture surfaces of flexure test specimens for the neat Polylite 31325 and bio-$CaCO_3$ /Polylite 31325 nanocomposites were

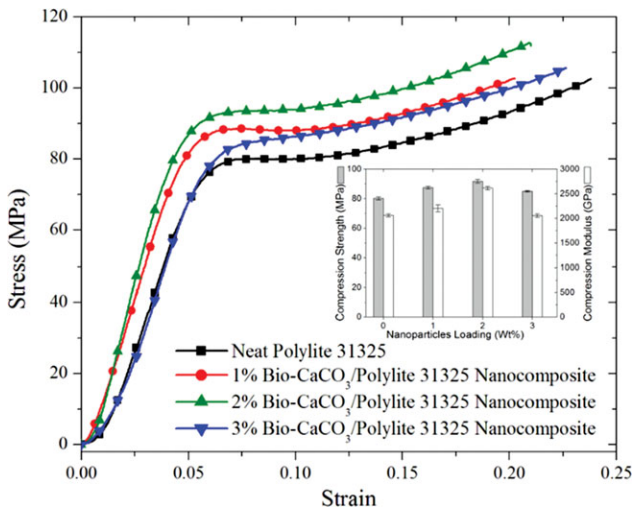

Figure 10. Quasi-static compression test results for neat Polylite 31325 and bio-$CaCO_3$/Polylite 31325 nanocomposite. Inset is a bar graph of compression results with error bars. [Color figure can be viewed in the online issue, which is available at wileyonlinelibrary.com.]

Table V. Quasi-Static Compression Tests Results for Neat Polylite 31325 and Bio-$CaCO_3$/Polylite 31325 Nanocomposites

No.	Sample	Compression strength (MPa)	Increase (%)	Compression modulus (GPa)	Increase (%)
1.	Neat Polylite	80.3 ± 1.1	-	2061.4 ± 29.1	-
2.	1% Bio-$CaCO_3$/Polylite	87.6 ± 0.9	9.1	2203.9 ± 71.7	6.9
3.	2% Bio-$CaCO_3$/Polylite	91.8 ± 1.2	14.3	2618.0 ± 34.7	27.0
4.	3% Bio-$CaCO_3$/Polylite	85.1 ± 0.4	6.0	2056.4 ± 33.8	−0.24

examined using SEM. During the test, it was observed that an initial crack occurred at the tension edge of all tested specimens. Figure 11 shows SEM micrographs for the fracture surfaces for (a) neat Polylite 31325 resin and (b, c, d) 1%, 2%, 3% bio-$CaCO_3$/Polylite 31325 nanocomposites, respectively. Neat Polylite 31325 resin exhibits a relatively smooth fracture surface and the SEM micrograph in Figure 11(a) indicates a typical fractography feature of brittle fracture behavior, thus, accounting for the low flexure strength of the unreinforced resin. The distance between two cleavage steps is about 10-20 μm, and the cleavage plane between them is flat and featureless. The fracture surfaces of the bio-$CaCO_3$/Polylite 31325 nanocomposites show considerably different fractographic features. For example, the failure surfaces of all nanocomposite samples are rougher compared to the neat Polylite 31325 samples.

Figure 11(b,c) show the fracture surfaces of 1% bio-$CaCO_3$/Polylite 31325 and 2% bio-$CaCO_3$/Polylite 31325, respectively. The surface roughness increased with higher bio-$CaCO_3$ content. Figures 11(b–d) also indicate that the size of the cleavage plane decreased with higher bio-$CaCO_3$ content. The micrographs of the fracture surfaces of the bio-$CaCO_3$/Polylite 31325 nanocomposites show that nanoparticles were uniformly dispersed in the resin. The flat cleavage planes were formed by the network of cleavage steps, and each plane contains an equal amount of the bio-$CaCO_3$ nanoparticles. During the failure process, the crack propagation changed direction as it crossed the bio-$CaCO_3$ nanoparticles. The bridge effect, which prevents crack opening, increased strength in the bio-$CaCO_3$/Polylite 31325 nanocomposites. The SEM micrograph in Figure 11(d) shows that the size of the cleavage plane decreased to ~5-10 μm after the infusion of the 3% bio-$CaCO_3$ nanoparticles. The decreased cleavage plane and the increased surface roughness imply that the path of the crack tip is distorted because of the bio-$CaCO_3$ nanoparticles, making crack propagation more difficult.

CONCLUSIONS

An effective fabrication method have been established to manufacture bio-nanocomposites using bio-inspired $CaCO_3$ nanoparticles derived from eggshells as nanofillers in Polylite 31325 thermoset polymer. XRD and TEM studies showed that using the non-contact mixing technique results in a good dispersion of bio-$CaCO_3$ nanoparticles in the polymer matrix and that the bio-nanoparticles were highly exfoliated in the polymer. Thermal analysis results have shown that the as-fabricated bio-nanocomposites are thermally more stable than their pristine

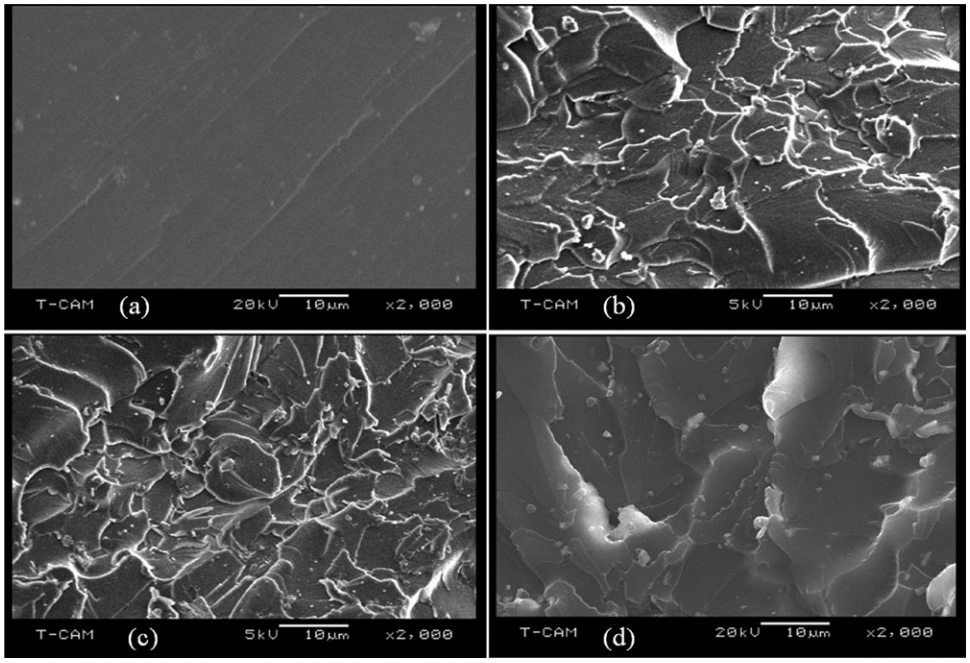

Figure 11. Fracture surfaces for (a) neat Polylite 31325 resin and (b–d) 1, 2, and 3% bio-$CaCO_3$/Polylite 31325, respectively.

counterparts indicating an increase in the cross-linking due to the incorporation of bio-$CaCO_3$ nanoparticles.

In addition mechanical tests indicate that there are major improvements in the mechanical properties. The investigation showed that 2% loading of bio-$CaCO_3$ nanoparticles demonstrated superior performance. This significant increase in the materials properties at low loadings of the nanofillers highlights the importance of this new class of bio-based materials to the industry, being particularly beneficial to the automotive sector where the continued need for material weight reduction must always be balanced with consideration of structural requirements.

ACKNOWLEDGMENTS

The authors would like to thank the National Science Foundation for their financial support through NSF-CREST#1137681, Alabama EPSCoR #1158862 and The Alabama Commission on Higher Education grants. The authors also would like to acknowledge the Reichhold, Inc., Research Triangle Park, NC, USA, for providing the Polylite® 31325-00 thermoset resin.

REFERENCES

1. Aldousiri, B.; Dhakal, H. N.; Onuh, S.; Zhang, Z. Y.; Bennett, N.; Richardson, M. O. W. *Compos. Part B-Eng.* **2012**, *43*, 1363.
2. Ha, S. R.; Rhee, K. Y.; Park, S. J.; Lee, J. H. *Compos. Part B-Eng.* **2010**, *41*, 602.
3. Toro, P.; Quijada, R.; Arias, J.; Yazdani-Pedram, M. *Macromol. Mater. Eng.* **2007**, *292*, 1027.
4. Masoodi, R.; El-Hajjar, R. F.; Pillai, K. M.; Sabo, R. *Mater. Des.* **2012**, *36*, 570.
5. Campanella, A.; La Scala, J. J.; Wool, R. P. *J. Appl. Polym. Sci.* **2011**, *119*, 1000.
6. Erman Senoz, E.; Stanzione, J. F.; Reno, K. H.; Wool, R. P.; Miller, M. E. *J. Appl. Polym. Sci.* **2013**, *128*, 983.
7. Mingjiang Zhan, M.; Wool, R. P. *J. Appl. Polym. Sci.* **2013**, *128*, 997.
8. Tsai, W.; Yang, J.; Hsu, H.; Lin, C.; Lin, K.; Chiu, C. *Micropor. Mesopor. Mat.* **2008**, *111*, 379.
9. Arias, J. L.; Fink, D. J.; Xiao, S. Q.; Heuer, A. H.; Caplan, A. I. *Int. Rev. Cytol.* **1993**, *145*, 217.
10. Arias, J. L.; Fernandez, M. S. *Mater. Charact.* **2003**, *50*, 189.
11. Lammie, D.; Baina, M. M.; Wess, T. *J. Synchrotron. Rad.* **2005**, *12*, 721.
12. Toro, P.; Quijada, R.; Yazdani, P.; Mehrdad, A.; Arias, J. L. *Mater. Lett.* **2007**, *61*, 4347.
13. Arias, J. L.; Quijada, R.; Toro, P.; Yazdani, P. US Patent, **2008**, No 7, 459,492 B2.
14. Ji, G.; Zhu, H.; Qi, C.; Zeng, M. *Polym. Eng. Sci.* **2009**, *49*, 1383.
15. Xu, Y.; Hanna, M. *Package Technol. Sci.* **2007**, *20*, 165.
16. Guo, Z.; Jones, A. G.; Li, N.; Germana, S. *Powder Technol.* **2007**, *171*, 146.
17. Isobe, T.; Kameshima, Y.; Nakajima, A.; Okada, K. *J. Eur. Ceram. Soc.* **2007**, *27*, 61.
18. Allaoui, A.; Hoa, S. V.; Pugh, M. D. *Compos. Sci. Technol.* **2008**, *68*, 410.
19. Rao, P.; Iwasa, M.; Tanaka, T.; Kondoh, I. *Ceram. Int.* **2003**, *29*, 209.
20. Rangari, V. K.; Hassan, T. A.; Mayo, Q.; Jeelani, S. *Compos. Sci. Technol.* **2009**, *69*, 2293.
21. Allaoui, S. V.; Hoa, M. D.; Pugh, M. *Comp. Sci. Tech.* **2008**, *68*, 410.
22. Takai, C.; Tsukamoto, M.; Fuji, M.; Takahashi, M. *J. Alloys Compoud* **2006**, *408*, 533.
23. Raoa, P.; Iwasa, M.; Tanaka, T.; Kondoh, I. *Ceram. Int.* **2003**, *29*, 209.
24. Ding, S. *J. Non-Cryst. Solids* **2007**, *353*, 2367.
25. Yamamoto, G.; Omori, M.; Yokomizo, K.; Hashida, T. *Diamond Related Mater.* **2008**, *17*, 1554.
26. Isobe, T.; Kameshima, Y.; Nakajima, A.; Okada, K. *J. Euro. Ceram. Soc.* **2007**, *27*, 61.
27. Gedanken, A. *Ultrason. Sonochem.* **2004**, *11*, 47.
28. Lee, J.; Ashokumar, M.; Kentish, S.; Grieser, F. *J. Phys. Chem. B* **2006**, *110*, 17282.
29. Jones, W. D.; Rangari, V. K.; Hassan, T. A.; Jeelani, S. *J. Appl. Polym. Sci.* **2010**, *116*, 2783.
30. Strong, A. Fundamentals of Composites Manufacturing: Materials, Methods and Applications, 1st Ed., Society of Manufacturing Engineers, **1989**.
31. Loera, A. G.; Cara, F.; Dumon, M.; Pascault, J. P. *Macromolecules* **2002**, *35*, 6291.
32. Rangari, V. K.; Koltypin, Y.; Cohen, Y. S.; Aurbach, D.; Palchik, O.; Felner, I. *J. Mater. Chem.* **2000**, *10*, 1125.
33. Cook, W. D.; Mehrabi, M.; Edward, G. H. *Polymer* **1999**, *40*, 1209.
34. Monstserrat, S. *J. Polym. Sci. Part B Polym. Phys.* **1994**, *32*, 509.
35. Monstserrat, S. *Polymer* **1995**, *36*, 435.
36. Ray, S.; Okamoto, K.; Okamoto, M. *Macromolecules* **2003**, *36*, 2355.
37. LeMay, J. D.; Kelley, F. N. *Adv. Polym. Sci.* **1987**, *78*, 115.
38. Gerard, J. F.; Galy, J.; Pascault, J. P.; Cukierman, S.; Halary, J. L. *Polym. Eng. Sci.* **1991**, *31*, 615.
39. Hiltz, J. A.; Keough, I. A. *Thermochim Acta* **1992**, *212*, 151.
40. Nielsen, L. E.; Landel, R. F. Mechanical Properties of Polymers and Composites; CRC Press; Rev and Expande edition, **1993**.
41. Kusy, R. P.; Whitley, J. Q. *Thermochim Acta* **1994**, *243*, 253.
42. Kalichevesky, M. T.; Jaroskiewicz, E. M.; Ablett, S.; Blanshard, J. M. V.; Lillford, P. J. *Carbohydr. Polym.* **1992**, *18*, 77.
43. Chatterjee, A.; Islam, M. *Mater. Sci. Eng. A* **2008**, *487*, 574.
44. Gupta, N.; Ricci, W. *Mater. Sci. Eng. A* **2006**, *427*, 331.